Natural variability in bee brain size and symmetry revealed by micro-CT imaging and deep learning

Philipp D. Lösel[1,2,#,*], Coline Monchanin[3,4,#,*], Renaud Lebrun[5,6], Alejandra Jayme[1,2], Jacob Relle[1,2], Jean-Marc Devaud[3], Vincent Heuveline[1,2,7,+], Mathieu Lihoreau[3,+]

[1] Engineering Mathematics and Computing Lab (EMCL), Interdisciplinary Center for Scientific Computing (IWR), Heidelberg University, Im Neuenheimer Feld 205, 69120 Heidelberg, Germany.
[2] Heidelberg Institute for Theoretical Studies (HITS), Schloss-Wolfsbrunnenweg 35, 69118 Heidelberg, Germany.
[3] Research Center on Animal Cognition (CRCA), Center for Integrative Biology (CBI); CNRS, University Paul Sabatier – Toulouse III, France.
[4] Department of Biological Sciences, Macquarie University, NSW, Australia.
[5] Institut des Sciences de l'Evolution de Montpellier, CC64, Université de Montpellier, Montpellier, France.
[6] BioCampus, Montpellier Ressources Imagerie, CNRS, INSERM, Université de Montpellier, 34090 Montpellier, France.
[7] Heidelberg University Computing Centre (URZ), Im Neuenheimer Feld 293, 69120 Heidelberg, Germany.

[#] Joint first authors
[+] Joint last authors
* Corresponding authors

Abstract

Analysing large numbers of brain samples is challenging but can reveal minor but statistically and biologically relevant variations, that provide important insights into animal behaviour, ecology and evolution. Here, we used micro-CT imaging and deep learning to perform automatic analyses of 187 bee brains (honey bees and bumblebees). This large-scale quantitative comparative analysis of 3D brain data revealed strong inter-individual variations in overall bee brain size that is consistent across colonies and species, suggesting selection processes supporting behavioural variability. In addition, analyses of bumblebee brains revealed a significant level of lateralization in the optic lobes, likely related to reported variations in visual learning. Our fast and accurate deep learning-based approach to process bee brain data is user friendly and holds considerable promises for conducting large-scale quantitative neuroanatomical comparisons across a wide range of species beyond insects. Ultimately, this will help address fundamental unsolved questions related to the evolution of animal brains and cognition.

Introduction

Artificial intelligence is revolutionising many areas of scientific research, helping scientists to examine large amounts of data, that are needed to address important open questions[1]. Neuroscience is a prominent example of a field that would greatly benefit from automated analysis tools for large-scale comparative investigations. In particular, animals, from insects to humans, show a rich diversity of behavioural profiles (or personalities) that may be underpinned by anatomical and cognitive variability[2]. Identifying natural variations in brain morphologies and performances between individuals can therefore help to understand the evolution of species and their potential for resilience in the widespread context of biodiversity loss[3]. However, such an approach currently requires extensive manual effort in order to obtain and analyse large and high-quality brain datasets, which typically limits investigations to a few individuals and to model species for which brain atlases are available (e.g. rodents[4], primates[5], *Drosophila*[6]). As a consequence, the scope for comparative research remains strongly restrained[7].

Three-dimensional (3D) imaging, in particular micro-computed tomography (micro-CT), now enables non-destructive, fine-scale imaging of internal structures of biological objects, such as brain tissues both *in vivo* and *ex vivo*. Recent improvements in resolution and acquisition times[8,9] have broadened its application to a wide range of animals, including non-model species of the smallest sizes, such as insects (e.g. ants[10,11], wasps[12,13], beetles[14,15], bees[16,17]). This facilitation of image acquisition has posed new demands for accelerated image analysis methods. A variety of user-friendly desktop and floor-standing devices has been made available. However, image segmentation and post-processing steps still require manual assistance[18–21], which is time-consuming (several hours or days to reconstruct a structure) and therefore not compatible with analyses of large datasets.

Here, we demonstrate how deep learning can considerably speed up 3D image analyses for large-scale comparative brain studies in non-model species. We illustrate our approach using the semi-automated[22,23] and automated segmentation methods integrated into the recently developed online platform Biomedisa[24] (https://biomedisa.org) to analyse micro-CT scan data from bee brains (Fig. 1). Despite its small size (<1 mm^3), the bee brain supports a puzzlingly rich behavioural repertoire that presents extensive inter-individual variability[25]. In social bees, such as honey bees and bumblebees, this variability is central to the division of labour that supports complex social organisations, and some of it has been associated with maturation of specific brain areas due to development and foraging experience[26,27]. This makes bees ideal models for studying insect cognitive functions and their underlying neural substrates[28,29]. However, there is still no clear link between possible differences in brain neuro-architecture and behavioural variance, as data from comparative analyses are missing. Studies are rare[30] and have worked on small samples (7[31] to 67[32] individuals). To fill this knowledge gap, we collected volumetric data on brains of 110 honey bees and 77 bumblebees and quantified variations in brain area volumes. For each species we used semi-automated segmentation to annotate the training data for a deep neural network, which was then used for subsequent automatic segmentation of the full dataset. This reduced data processing time by approximately up to 98% compared to a conventional manual segmentation approach. Our approach

revealed size variations across brain samples as well as strong anatomical asymmetries, supporting behavioural observations.

Results & Discussion

Automatic segmentation of bee brains considerably speeds up analysis.

We performed micro-CT scanning of 120 forager honey bees (*Apis mellifera,* Buckfast) from two apiaries (Population A: 100 bees from 6 hives, population B: 20 bees from 3 hives) in Toulouse (France). Brain samples were prepared following Smith et al.[17] and CT-scanned at a resolution of 5.4 µm isotropic voxel size (see "Methods"). Among the 120 micro-CT scanned brains, 10 were damaged during manipulation and discarded, leaving 110 brains for our analysis. Image dimensions and image spacing varied across subjects and averaged 844×726×485 isotropic voxels and 0.0054×0.0054×0.0054 mm^3, respectively.

We analysed six major brain areas (without cell bodies) based on the 3D bee brain atlas[33]: the antennal lobes (AL) that receive olfactory information from the antennae; the mushroom bodies (MB, each comprising the medial and lateral calyces, peduncle and lobe) that integrate olfactory and visual information; the central complex (CX, comprising the central body, the paired noduli and the protocerebral bridge) that receives compass and optic flow information; the medullae (ME) and lobulae (LO) that receive visual information from the compound eyes, together combined as 'optic lobes' (OL, retinae and laminae were not measured); and the other remaining neuropils (OTH) (including protocerebral lobes and subesophageal zone) (Fig. 2). ALs and OLs are involved in olfactory and visual processing, respectively, while the CX and MBs play important roles in locomotor behaviour, learning and memory, respectively[34].

The volumetric analysis of the different neuropils required their isolation from the CT scans by segmentation (Figs. 1, 2). For better automatic segmentation (Fig. 3), each dataset was manually cropped to the area of the neuropils (Fig. 2d) using AVIZO 2019.1, resulting in an average size of 451 ×273×167 voxels. For automatic segmentation, we used the deep neural network interface from the online platform Biomedisa. To train a deep neural network, Biomedisa needs a set of fully segmented volumetric images. To create the first three datasets, labels were assigned manually to the six neuropils in every 10th slice and every 5th slice in the interval containing CX within the 3D volume using AVIZO 2019.1 (Thermo Fisher Scientific, Waltham, USA). For better performance compared to purely morphological interpolation (see "Methods" and Fig. 3), Biomedisa's semi-automatic smart interpolation was used to segment the remaining volume between the pre-segmented slices. Before interpolation, the image data was slightly smoothed using Biomedisa's denoise function (see "Methods"). Subsequently, outliers (i.e. unconnected voxels or islands) were removed and segmentation errors were corrected manually by an expert using AVIZO 2019.1.

Additional training data was then iteratively created using neural networks. Starting from three semi-automatically segmented images, we trained neural networks on 3, 7, 12, 18, and 26 images by adding manually corrected segmentation results of the last trained network to the training

data after each step (Fig. 1). In all cases, the network's default configuration was used (see "Methods"). The corresponding training times on 4 NVIDIA Tesla V100s were 1.5, 3.5, 6, 9, and 13 hours. At this point, segmentation accuracy could no longer be significantly improved by additional training data (Fig. 3 and Supplementary Table 1). We finally used the network trained on the set of 26 images ("training images") to automatically segment the remaining 84 micro-CT scans of honey bee brains ("test images"). The automatic segmentation of each 3D image took an average of 16 seconds using an NVIDIA RTX A5000 or 82 seconds using an Intel® Core™ i9-11900K Processor. All segmentation results were checked and manually corrected by an expert (using 'remove islands' and 'merge neighbours' functions in AVIZO 2019.1).

To test the suitability of our approach to brain datasets from other species, we also performed micro-CT scanning of 77 bumblebees (*Bombus terrestris*) from 4 commercially-available colonies (colony A: 18 bumblebees, colony B: 20 bumblebees, colony C: 21 bumblebees, colony D: 18 bumblebees). Based on the evaluation for an increasing number of training images (see "Methods", Fig. 3 and Supplementary Table 1), we decided to semi-automatically segment 13 training images (which we considered to be a good balance between manual effort and accuracy) using Biomedisa to train a neural network on the bumblebee dataset. The trained network was then used to automatically segment the remaining 64 bumblebee CT scans.

Overall, AVIZO 2019.1 was used for pre-segmentation, correction of segmentation results and measurement of absolute neuropil volumes calculated with the voxel count function. Biomedisa was used for smart interpolation to create the initial training data, training of deep neural networks and subsequent automatic segmentation. Since Biomedisa supports the AMIRA Mesh File format, deployed by AVIZO and AMIRA, data can be easily transferred between the Biomedisa online platform and AVIZO 2019.1. In addition to AMIRA meshes (AM), Biomedisa supports many other common data formats (such as DICOM, NifTI, TIFF, NRRD, MHA, MHD) and can also be used in combination with other segmentation tools. For both datasets, this automatic segmentation considerably reduced the time and effort required for image analysis compared to purely manual segmentation. For each 3D image, it took about 5 to 10 minutes for the whole procedure: importing the data into AVIZO 2019.1, cropping to the area of the neuropils, exporting the data, uploading it to Biomedisa, performing automatic segmentation, downloading and importing the segmentation result into AVIZO 2019.1, correcting the segmentation result manually, and measuring volumes. In contrast, a purely manual or semi-automatic approach would have taken several hours for each CT scan (approx. 5 to 6 h using conventional manual segmentation and 2 to 3 h using Biomedisa's semi-automatic segmentation). Depending on the quality of the automated segmentation result, either no correction was required (Supplementary Fig. 1a) or manual correction typically took 1 to 2 minutes (Supplementary Fig. 1b), rarely longer if the result was significantly flawed (Supplementary Fig. 1c). Typical artefacts resulting from the automatic segmentation are outliers (Supplementary Fig. 1b) which can be easily removed either with Biomedisa's cleaning function or with AVIZO 2019.1. Overall, with this approach, the manual effort for segmenting the full honey bee dataset (15 to 27 h) was about

95 to 98% less than purely manual segmentation (550 to 660 h) and about 87 to 93% less for the bumblebee dataset (31 to 50 h compared to 385 to 462 h).

Automatic segmentation of bee brains is highly accurate.

To evaluate the accuracy of the automatic segmentation, two complementary and commonly applied metrics for measuring performance in biomedical image segmentation challenges were used[35] (see "Methods"): the Dice similarity coefficient (Dice) and the average symmetric surface distance (ASSD). The Dice score quantifies the matching level between two segmentations and is between 0 (no overlap at all) and 1 (perfect match). The ASSD is the average 3D Euclidean distance from a point on the surface of one segmentation to the closest point on the surface of the second segmentation and vice versa. The smaller the ASSD, the closer the two segmentations.

For both bee species, we measured the accuracy of the segmentation results of the test images performed by the deep neural network trained with the respective training data. We compared the results obtained without further manual post-processing with ground truth data generated by an expert (i.e. segmentation results after revision and manual correction). For the automatic segmentation of the 84 honey bee brains, a Dice score of 0.988 was achieved (Supplementary Table 1). In 10.7% of the test images, little or no manual correction was necessary (error less than 0.01% of Dice score, Supplementary Fig. 1a). In 84.5%, a slight manual correction was required taking 1 to 2 minutes (error ranging between 0.01% and 4%, Supplementary Fig. 1b). Only 4.8% of the segmentation results were significantly flawed (error greater than 4%, Supplementary Fig. 1c), usually due to a significant deviation from the training data (e.g. images from incompletely stained or damaged brains during tissue processing) and required extensive manual correction or semi-automatic reconstruction using Biomedisa's smart interpolation. For the automatic segmentation of the 64 bumblebee brains, a Dice score of 0.983 was achieved (Supplementary Table 1). Here, no error was less than 0.01%. However, for 9.4% of the segmentation results, the error was less than 0.1%. For 78.1% it was between 0.1% and 4% and 12.5% had an error greater than 4%.

Biomedisa thus enabled high-precision and fast segmentation of the 148 test images (84 honey bee, 64 bumblebee), which required manual correction of the segmentation results equalling a Dice score of 0.012 (i.e. an error of 1.2%) for the honey bee brains and 0.017 for the bumblebee brains (Supplementary Table 1). Note that major corrections were mostly only required for CX (an average error of 3.3% for honey bees and 16.3% for bumblebees), because its fine structure combined with low contrast often makes it difficult to detect this neuropil, particularly in the bumblebee CT scans.

Brain volumes varied significantly among honey bees.

To validate our approach, we compared our results with previously published data, focusing on the volumes of the six neuropils considered (Fig. 4) in honey bees. Division of labour in honey bee colonies is primarily based on age differences among individuals[36]. Since workers vary little in body size[37], it was expected that their brain volume would also show only small variation. Our results are

broadly consistent with previous studies based on smaller datasets[27,31–33,38–44] and using different quantitative approaches (CT scan data[43,44], or stereo[27,31,32,40], confocal[33,38,39], and nuclear magnetic resonance[39] microscopy). When data do not match, we expect our measures to be more accurate than those in previous studies since they were obtained from thinner slices (5.4 µm vs. 8[33] to 60[41] µm) and measurements were taken on all successive slices, rather than leaving intermediate slices aside and using linear interpolation (e.g. Cavalieri principle[45]). Such technical discrepancies likely explain under- or over-estimated volumes in other studies compared to ours. Also note that some measurements from other studies have uncertainties, e.g. a precise description of which structures were included in the measurement of CX[33] or whether or not cell bodies were included in the total brain volume[31]. Additionally, differences in the estimated structural volumes may arise from biological differences among samples taken from bees of different subspecies (e.g. European and Africanized honey bees[32]), ages and foraging experiences of individual bees[27,42].

Among the 110 honey bee brains, total brain volume (i.e. sum of all measured neuropils) varied by 32% and neuropil volumes by 29 to 52% (Fig. 4 and Table 1). We found strong positive correlations between the absolute volumes of all neuropils but CX and total brain volume (Fig. 5a−g). Most neuropils scaled isometrically with total brain volume (Fig. 5h), with only a lower correlation coefficient for CX (R^2=0.36, $p<0.001$; Fig. 5f). This is coherent with the results of the largest comparative analysis of honey bee brains so far (121 brain samples obtained by electron microscopy technique in two honey bee strains)[32]. When considering relative volumes (ratio of neuropil volume to total brain volume), we only found a weak correlation between AL and total brain volumes (Supplementary Fig. 2a).

When assessing correlations between absolute volumes across neuropils, we found strong correlations between OL, LO and ME volumes (Supplementary Table 2), as previously reported[32]. In our dataset, however, AL volume is positively correlated with all other neuropils. We also found positive correlations for MB, CX and OTH with all other neuropils, except between MB and CX, which were not correlated. We next compared the relative neuropil volumes in order to search for relevant allometric relationships (Supplementary Table 2). Again, we found strong correlations between the relative volumes of OL, LO and ME, consistent with previous studies[32]. In addition, the relative volume of AL correlates positively with those of OL, ME, and LO, while previous work on honey bees[32] and other bee species[46] suggested a negative correlation between AL and OL as a possible trade-off between visual and olfactory processing. Also, the relative OTH volume was negatively correlated with all other neuropils, with the exception of CX. Therefore, honey bees with larger brains tend to have larger neuropils overall, with the exception of CX, whose size is not as strongly related to brain size as the other neuropils. This weaker correlation could also be due to the small size of the neuropil and potential measure uncertainties caused by the difficulty of its segmentation.

Variance in honey bee brain volumes was similar within and between colonies.

Next, we explored the distribution of honey bee brain volumes within and between colonies. Social insect colonies can be considered superorganisms, characterised by a division of labour among

workers that is partly determined by the genetics, age and morphology of individuals[47]. In honey bees, MB volume increases with age[27] and foraging experience[42,48] and AL volume correlates with behavioural tasks (i.e. nurse, comb-builder, nectar or pollen forager)[49]. These variations are thought to support division of labour, as larger volumes (relative and/or absolute) of specific neuropils may allow some individuals to be more efficient at certain tasks, or result from behavioural specializations. For example, larger ALs and/or MBs may provide foragers with better abilities at learning spatial information and floral cues than in-hive workers[42]. While some studies investigated variations in brain size between species[31] or intra-species variations due to stress exposure (e.g. pesticides[16], nutrition[38]), to our knowledge, the magnitude of intra- and inter-colony variability under standard conditions has not yet been investigated. Stable within-hive variation in brain volumes across colonies with different genetic backgrounds and in different geographic areas would suggest selection for variability.

Honey bees in the nine colonies exhibited overall similar average brain volumes (F-test: $p=0.428$; Fig. 6a and Table 1), hence, inter-colony differences do not explain the substantial (32%) inter-individual variability. Within colonies, the values were also relatively stable (Supplementary Table 3). However, several neuropils exhibited significant variations in their absolute volumes across colonies (Fig. 6b−g and Table 1): AL (F-test: $p<0.001$; Fig. 6b), MB (F-test: $p=0.025$; Fig. 6c), OL (F-test: $p<0.001$; Fig. 6d) and LO (F-test: $p=0.009$; Fig. 6f). Interestingly, intra-colony variability of neuropils was generally lower and CX and OTH were the more variable (resp. 11 to 49% and 11 to 51%, depending on the colony), despite non-significant changes between colonies (Supplementary Table 3 and Fig. 6g−h). Notably, we only found low intra-colonial variations in MB volumes (7 to 30%), which are known to increase in size by 15% with age and foraging experience over the lifespan[27]. This low level of variability is probably due to the fact that we only studied forager bees (see 'Methods') and therefore could not reflect the reported brain plasticity between emerging, nurse and forager bees.

Thus, overall, we found moderate variability in brain size and neuropil volumes, which were rather stable within colonies, based on a relatively homogeneous sample in terms of strain (Buckfast) and behavioural specialization (foragers). This suggests adaptive levels of brain size variation, potentially underpinning behavioural diversity in division of labour, particularly when specific brain areas are considered.

Bumblebees show higher variability in brain and neuropil volumes than honey bees.

To illustrate how our approach can be used to compare species and to demonstrate its generalisability to other sample series, we applied the same analyses to the bumblebee brains. Bumblebees have become important model organisms, complementing honey bees in behavioural and cognitive research[50], and for which a brain atlas was recently published[51]. In contrast to honey bees, division of labour in bumblebees is primarily based on body size variation[52] with little effect of age (foragers tend to be larger than non-foragers[53]). Therefore, it is not surprising that overall bumblebees exhibited higher variation levels in total brain volume (52%; Fig. 7a and Supplementary

Table 4) and neuropil volumes (44 to 85%; Fig. 7b−h), as compared to honey bees. Note, however, that the 77 bumblebees randomly sampled in the four source colonies were likely to be more heterogeneous than the 110 honey bees, which were only foragers. Yet, all neuropils scaled isometrically with total brain volume (Fig. 7i), with again only a lower correlation for CX (R^2=0.59, p<0.001). In contrast to honey bees, where only the relative volume of AL was weakly correlated with total brain volume, the relative volumes of OL, ME (and consequently LO) were negatively correlated with total brain volume, while the relative volume of OTH was positively correlated (Fig. 7j).

Regarding correlations between neuropil volumes (Supplementary Table 5), we found significant and strong positive correlations for all possible permutations in absolute volumes. Relative volumes showed the same major trends as in honey bees (Supplementary Table 5): OL, ME and LO were positively correlated with each other, OTH was negatively correlated with all other neuropils, except CX, and relative AL volume was positively correlated with MB, OL, ME and LO relative volumes. Overall, it seems that the larger the brain, the larger the proportion of OTH and the relatively smaller the other neuropils.

The four bumblebee colonies examined in this study did not show significant differences for any of the neuropil volumes, except for LO (Supplementary Table 4), while we found volume differences for AL, MB, OL and LO when comparing honey bee colonies (Table 1 and Fig. 6). Again, this is not surprising since the bumblebee sample was more heterogeneous in terms of individual size than the sample of forager honey bees. Thus, like for honey bees, we found relatively stable intra-colony variability in brain and neuropil volumes (Supplementary Table 4).

Optic lobes show left-right asymmetry in bumblebees but not in honey bees.

Taking advantage of having an unprecedentedly large number of complete bee brain volumes, we finally explored potential asymmetries in the paired structures of honey bee and bumblebee brains. Bees show lateralized learning abilities[54,5558]. However, no study has reported asymmetries in brain size that might reveal neural adaptations supporting the behavioural observations[57,59]. We therefore compared the left and right volumes of all paired neuropils (Table 1, Fig. 8 and Supplementary Table 4). Note that left and right MB structures were often difficult to separate, resulting in the comparison of the two MB sides being based only on 59 honeybees and 36 bumblebees, respectively.

For honey bee brains, we found no lateral differences in the absolute volumes of AL (LMM: p=0.324), MB (LMM: p=0.243), ME (LMM: p=0.964), LO (LMM: p=0.285) and OL (LMM: p=0.736). We did not find any significant difference in the relative volume of AL (LMM: p=0.341), MB (LMM: p=0.338), ME (LMM: p=0.907), LO (LMM: p=0.245) and OL (LMM: p=0.665) neither. Thus overall, there were no anatomical left-right differences in the honey bee brain. By contrast, the same analysis revealed some asymmetry in bumblebee brains. There was no difference in the lateral absolute volumes of AL (LMM: p=0.179) and MB (LMM: p=0.664). However, the left ME (LMM: p=0.019) and left LO were significantly smaller (LMM: p=0.002) in 38% and 34% respectively of the brains, resulting in an overall smaller left OL (LMM: p=0.005) (Fig. 8). Relative lateral volumes of AL (LMM: p=0.237) and MB (LMM: p=0.864) were similar. The relative volume of the left ME (LMM: p=0.015) and left LO

(LMM: p=0.001) were smaller, resulting in the left OL having a smaller relative volume than the right side (LMM: p=0.004) in 38% of the brains.

Surprisingly, we found no evidence of volumetric asymmetries in honey bees that could be correlated with the improved learning performances in the olfactory[43] and visual[54] modalities using the right side. This may be either because left-right differences in ALs or OLs were too small to reach significance in our sample, or because the larger number of olfactory sensillae on the right antenna[43] does not go along with neuropil size differences (whether the right eye has larger ommatidia remains to be determined). This might be different in bumblebees: while the right-sided dominance for olfactory learning, also observed in this species, also seems to be related to a peripheral asymmetry (more sensillae on the right antenna[56]) rather than a central one (our observations), this may not be the case for vision. Indeed, our study allows to predict possible visual lateralization as well, which still needs to be demonstrated. Since the OL processes visual information[57], a larger OL on the right could provide greater computational capacity and thus explain why bees perform better with their right eyes. Alternatively, if visual learning preferentially solicits the right visual pathway, a larger right OL might be a consequence of more pronounced activity-driven structural changes (e.g. synapse production).

Conclusion.

Comparative analyses of animal brain volumes are currently limited to a few individuals in model species[58]. Here we showed how deep neural networks can be used for fast and accurate analysis of large amounts of volumetric brain images, opening new possibilities for broad comparative analyses in insects and invertebrates in general. Our results on honey bees and bumblebees show high natural variability in brain area sizes that is stable across colonies, suggesting selection for variability supporting adaptive division of labour. Brain asymmetries may also explain previously reported behavioural lateralization[59,60]. Future combination of brain and behavioural analyses using our method for automated image segmentation will help address important open and hotly debated questions related to neuroscience and cognition. Are bigger brains more performant[61,62]? What are the influences of social and ecological factors in brain evolution[2]? What is the effect of environmental stressors on brain development and cognition[16]? Importantly, Biomedisa is accessible via a web browser and does not require complex or tedious software configuration or parameter optimisation, making it user-friendly even for biologists with no substantial computational expertise. We therefore expect our approach to be widely used to study the evolution of animal body parts or organs, beyond the brain itself. Indeed, Biomedisa is suitable for many types of volumetric image data other than micro-CT scans, e.g. from confocal laser scanning microscopy (CLSM), focused ion beam scanning electron microscopy (FIB-SEM), histological imaging, or magnetic resonance imaging (MRI), which offer the opportunity for a wide range of studies in biology, ecology and evolution to perform large-scale, cost-effective and time-efficient analyses.

Methods

Sample preparation and CT scan.

We performed micro-computed tomography scanning of honey bees (*Apis mellifera,* Buckfast) and bumblebees (*Bombus terrestris*). Honey bees were collected from 9 hives located in two apiaries around Toulouse, France, in August 2020 (Population A (GPS coordinates: 43.55670, 1.47073): 100 bees from 6 hives; population B (43.26756, 2.28376): 20 bees from 3 hives). Foragers returning to the colony were collected at the hive entrance, frozen and stored at -18°C. Bumblebees were purchased from a commercial supplier (Koppert, France) and 77 workers were collected from 4 colonies and frozen at -18°C. For staining bee brains, we removed the front cuticle just above the mandibles and submerged the heads in phosphotungstic acid (5% in a 70/30% ethanol/water solution) for 15 days at ambient temperature[17]. The staining agent is non-hazardous and does not lead to overstaining of the soft tissues, in contrast to other compounds previously used in CT scan studies of insect brains such as osmium-tetroxide[44] or iodine[63]. Two heads were scanned at the same time (as both fit in the field of view of the flat-panel imager) using the micro-CT station EasyTom 150/RX Solutions (Montpellier Ressources Imagerie, France), with the following parameters: resolution of 5.4 µm isotropic voxel size, 40 kV, 130 µA, 736 radiographic projections (acquisition time: 15 minutes). Raw data for each brain scan was reconstructed using X-Act software (RX Solutions, Chavanod, France). The reconstructed volumes were then re-oriented to the same (frontal) plane-of-view and each brain was re-sliced into a new series of two-dimensional images.

Statistical analysis.

We analysed the parameters obtained from the reconstructed neuropils using R Studio v.1.2.5033[64]. We assessed correlations between brain neuropil volumes using the *rcorr* function from the *Hmisc* package[65]. To analyse the inter-colonial variations of brain volume, we conducted linear mixed models (LMMs) using the *lme4* package[66], with hive as fixed effect and population as random factor. LMMs were followed by F-tests to test the significance of fixed categorical variables using the *anova* function in the *car* package[67]. To assess the potential lateralization of paired neuropils, we conducted Student's t-Test using Python's SciPy library.

Artificial neural network architecture.

Biomedisa uses Keras with TensorFlow backend. A patch-based approach is utilized in which 3D patches of the volumetric images are used instead of the entire CT scan. The patches serve as input for a 3D U-Net and have a size of 64×64×64 voxels. Before extracting the patches, images are scaled to a size of 256×256×256 voxels and transformed to have the same mean and variance. An overlapping of the patches is achieved by a stride size of 32 pixels that can be configured in Biomedisa. The network architecture of the deep neural network follows the typical architecture of a 3D U-Net[68]. It consists of a contracting and an expansive part with a repeated application of two 3×3×3 convolutions, each followed by batch normalisation and a rectified linear unit (ReLU) activation

layer. Each contracting block is followed by a 2×2×2 max pooling operation with stride size of 2 for downsampling. At each downsampling step, the number of feature channels is doubled, starting with 32 channels. Every step in the expansive part consists of an upsampling of the feature map and a concatenation with the corresponding cropped feature map from the contracting path, followed by two 3×3×3 convolutions, with each followed by batch normalisation and a ReLU activation layer. At the final layer, a 1×1×1 convolution is used to map each feature vector to the desired number of labels. To train the network, stochastic gradient descent is used with a learning rate of 0.01, decay of 1×10^{-6}, momentum of 0.9, enabled Nesterov momentum, 200 training epochs, and a batch size of 24 samples.

Removing outliers.

To evaluate the segmentation results, Biomedisa's cleanup function was used for all neuropils except CX to automatically remove outliers or islands with a threshold of 0.1. This threshold value was set lower than the standard configuration (0.9) in order to avoid a partial deletion of paired neuropils.

Evaluating the creation of training data.

To evaluate the semi-automatic segmentation used to create the labels for the training images, we compared the commonly used linear interpolation in AVIZO 2019.1 and the smart interpolation in Biomedisa using the set of 26 training images. For intervals including CX we used every 5th slice of the ground truth data, otherwise every 10th slice as initialisation. Using the same pre-segmented slices, Biomedisa's smart interpolation, which also takes into account the underlying image data, achieves higher segmentation accuracy (average Dice score of 0.967) compared to the purely morphological interpolation of AVIZO 2019.1 (average Dice score of 0.928, Fig. 3 and Supplementary Table 1). Thus, the manual work required to create the training data for a neural network is significantly reduced.

Increasing the number of training images.

To test the performance of the automatic segmentation in terms of the number of training images, we evaluated the accuracy of the trained network using 3 to 26 training images (Fig. 3 and Supplementary Table 1). Here, the 110 honey bee images and the corresponding labels were split into 26 training images, 30 validation images and 54 test images. The accuracy of the training process, measured using the Dice score, was evaluated using the validation data after each of the 200 epochs performed. Only the best performing network was saved. Finally, the trained network was applied to the 54 test images and the average Dice score of the segmentation results was calculated. While increasing the number of training images improves the accuracy of the automatic segmentation and thus reduces the required manual post-processing, this improvement gradually slows down with an increasing number of training images. Therefore, one has to weigh the gain in accuracy against the

additional effort required. Using the honey bee dataset, 12 to 20 training images are sufficient for adequate automatic segmentation.

Uncropped image data.

The network was also trained and evaluated using uncropped images (i.e. original honey bee CT scans). Cropping the image data to the area of the neuropils significantly increased the segmentation accuracy of the neural network from a total Dice score of 0.928 for the uncropped images to 0.970 for the cropped image data (Fig. 3 and Supplementary Table 1). By default, Biomedisa scales each image to a size of 256 pixels for each axis to facilitate training. The cropped image data (average size of 451×273×167 voxels) were thus scaled with an averaged factor of 0.57 and 1.53 along the x- and z-axes, and only marginally along the y-axis. Without cropping the image data (average size of 844×726×485 voxels), a large amount of redundant information is added to the training data. In addition, the loss of resolution due to the scaling of the image is significantly larger compared to cropped image data.

Automatic cropping.

As an alternative to manual cropping, a neural network can be trained with Biomedisa to automatically crop the image data to the region of interest before segmentation. Here the DenseNet121[69] pre-trained on the ImageNet database is used to decide whether a slice of the volume contains the object or not. Applying the network to all three axes creates a bounding box covering the honey bee brain. Adding a buffer of 25 slices to all sides after cropping ensures that the entire object is within the bounding box. The network is trained in two steps. First, the head of the pre-trained network is removed and replaced with a global average pooling layer, a dropout layer with a probability of 0.3 to avoid overfitting, and a final dense layer with sigmoid activation function. The weights of the base model are kept fixed while the head is optimised with binary cross-entropy, Adam optimiser with a learning rate of 0.001 and 50 epochs. Second, the entire DenseNet121 is fine-tuned to the honey bee training data with a learning rate of 1×10^{-5} and 50 epochs. Auto-cropping achieves a Dice score of 0.952, which increases accuracy by 2.4% compared to uncropped honey bee image data (Fig. 3 and Supplementary Table 1).

Evaluation metrics.

For two segmentations X and X' consisting of n labels, the Dice similarity coefficient (Dice) is defined as

$$\mathrm{Dice} = \frac{2\sum_{i=1}^{n}|X_i \cap X_i'|}{|X| + |X'|},$$

where $|X|$ and $|X'|$ are the total number of voxels of each segmentation, respectively, and X_i is the subset of voxels of $|X|$ with label i. For the surfaces S_i and S_i' of the two segmentations, the average symmetric surface distance (ASSD) is defined as

$$\mathrm{ASSD} = \frac{1}{|S| + |S'|} \sum_{i=1}^{n} \left(\sum_{p \in S_i} d(p, S'_i) + \sum_{p' \in S'_i} d(p', S_i) \right),$$

where

$$d(p, S'_i) = \min_{p' \in S'_i} \|p - p'\|_2$$

is the Euclidean distance from a point p on the surface S_i of label i to the closest point p' on the corresponding surface S'_i of the second segmentation.

Denoising image data.

Volumetric images are denoised using an arithmetic mean filter

$$A(x, y, z) = \frac{1}{|M|} \left(\sum_{i,j,k \in M} I(i, j, k) \right)$$

with a filter mask *M* of 3×3×3 voxels.

Data availability

The honey bee dataset, bumblebee dataset and trained networks are available at https://biomedisa.org/gallery/. Further data will be made available by the corresponding authors upon reasonable request.

Code availability

The source code is available as part of the Biomedisa open source project. It was developed and tested for Ubuntu 20.04 LTS and Windows 10. Biomedisa can be used via the command line or with any common browser as an interface. The source code can be downloaded from https://github.com/biomedisa/biomedisa/ and installed according to the installation instructions.

References

1. Appenzeller, T. The AI revolution in science. *Science* **357**, 16–17 (2017).
2. Dunbar, R. I. M. The social brain hypothesis. *Evol. Anthropol. Issues News Rev.* **6**, 178–190 (1998).
3. Cardinale, B. Impacts of biodiversity loss. *Science* **336**, 552–553 (2012).
4. Kumazawa-Manita, N., Katayama, M., Hashikawa, T. & Iriki, A. Three-dimensional reconstruction of brain structures of the rodent *Octodon degus*: a brain atlas constructed by combining histological and magnetic resonance images. *Exp. Brain Res.* **231**, 65–74 (2013).
5. Newman, J. D. *et al.* A combined histological and MRI brain atlas of the common marmoset monkey, *Callithrix jacchus*. *Brain Res. Rev.* **62**, 1–18 (2009).
6. Rein, K., Zöckler, M., Mader, M. T., Grübel, C. & Heisenberg, M. The *Drosophila* standard brain. *Curr. Biol.* **12**, 227–231 (2002).
7. Healy, S. *Adaptation and the brain*. (Oxford University Press, 2021).
8. dos Santos Rolo, T., Ershov, A., van de Kamp, T. & Baumbach, T. In vivo X-ray cine-tomography for tracking morphological dynamics. *Proc. Natl. Acad. Sci.* **111**, 3921–3926 (2014).
9. Maire, E. & Withers, P. J. Quantitative X-ray tomography. *Int. Mater. Rev.* **59**, 1–43 (2014).
10. Hita Garcia, F., Fischer, G., Liu, C., Audisio, T. L. & Economo, E. P. Next-generation morphological character discovery and evaluation: an X-ray micro-CT enhanced revision of the ant genus *Zasphinctus* Wheeler (*Hymenoptera, Formicidae, Dorylinae*) in the Afrotropics. *ZooKeys* **693**, 33–93 (2017).
11. Richter, A. *et al.* Comparative analysis of worker head anatomy of Formica and Brachyponera

(Hymenoptera: Formicidae). *Arthropod Syst. Phylogeny* **78**, 133–170 (2020).
12. Pasandideh Saqalaksari, M., Talebi, A. A. & van de Kamp, T. MicroCT 3D reconstruction of three described braconid species (Hymenoptera: Braconidae). *J. Insect Biodivers. Syst.* **6**, 331–342 (2020).
13. van de Kamp, T. *et al.* Parasitoid biology preserved in mineralized fossils. *Nat. Commun.* **9**, 3325 (2018).
14. Li, D., Zhang, K., Zhu, P., Wu, Z. & Zhou, H. 3D configuration of mandibles and controlling muscles in rove beetles based on micro-CT technique. *Anal. Bioanal. Chem.* **401**, 817–825 (2011).
15. van de Kamp, T. *et al.* Comparative thorax morphology of death-feigning flightless cryptorhynchine weevils (Coleoptera: Curculionidae) based on 3D reconstructions. *Arthropod Struct. Dev.* **44**, 509–523 (2015).
16. Smith, D. B. *et al.* Insecticide exposure during brood or early-adult development reduces brain growth and impairs adult learning in bumblebees. *Proc. R. Soc. B Biol. Sci.* **287**, 20192442 (2020).
17. Smith, D. B. *et al.* Exploring miniature insect brains using micro-CT scanning techniques. *Sci. Rep.* **6**, 21768 (2016).
18. Dumbravă, M. D. *et al.* A dinosaurian facial deformity and the first occurrence of ameloblastoma in the fossil record. *Sci. Rep.* **6**, 29271 (2016).
19. Gross, V. *et al.* X-ray imaging of a water bear offers a new look at tardigrade internal anatomy. *Zool. Lett.* **5**, 14 (2019).
20. Jones, M. E. H., Button, D. J., Barrett, P. M. & Porro, L. B. Digital dissection of the head of the rock dove (Columba livia) using contrast-enhanced computed tomography. *Zool. Lett.* **5**, 17 (2019).
21. Pardo, J. D., Szostakiwskyj, M., Ahlberg, P. E. & Anderson, J. S. Hidden morphological diversity among early tetrapods. *Nature* **546**, 642–645 (2017).
22. Lösel, P. & Heuveline, V. Enhancing a diffusion algorithm for 4D image segmentation using local information. in *Medical Imaging 2016: Image Processing* vol. 9784 97842L (International Society for Optics and Photonics, 2016).
23. Lösel, P. D. GPU-basierte Verfahren zur Segmentierung biomedizinischer Bilddaten. (Heidelberg University, 2022).
24. Lösel, P. D. *et al.* Introducing Biomedisa as an open-source online platform for biomedical image segmentation. *Nat. Commun.* **11**, 5577 (2020).
25. Jandt, J. M. *et al.* Behavioural syndromes and social insects: personality at multiple levels. *Biol. Rev.* **89**, 48–67 (2014).
26. Fahrbach, S. E., Moore, D., Capaldi, E. A., Farris, S. M. & Robinson, G. E. Experience-expectant plasticity in the mushroom bodies of the honeybee. *Learn. Mem.* **5**, 115–123 (1998).
27. Withers, G. S., Fahrbach, S. E. & Robinson, G. E. Selective neuroanatomical plasticity and division of labour in the honeybee. *Nature* **364**, 238–240 (1993).
28. Giurfa, M. Cognition with few neurons: higher-order learning in insects. *Trends Neurosci.* **36**, 285–294 (2013).
29. Menzel, R. The honeybee as a model for understanding the basis of cognition. *Nat. Rev. Neurosci.* **13**, 758–768 (2012).
30. Sombke, A., Lipke, E., Michalik, P., Uhl, G. & Harzsch, S. Potential and limitations of X-Ray micro-computed tomography in arthropod neuroanatomy: a methodological and comparative survey. *J. Comp. Neurol.* **523**, 1281–1295 (2015).
31. Gowda, V. & Gronenberg, W. Brain composition and scaling in social bee species differing in body size. *Apidologie* **50**, 779–792 (2019).
32. Gronenberg, W. & Couvillon, M. J. Brain composition and olfactory learning in honey bees. *Neurobiol. Learn. Mem.* **93**, 435–443 (2010).
33. Brandt, R. *et al.* Three-dimensional average-shape atlas of the honeybee brain and its applications. *J. Comp. Neurol.* **492**, 1–19 (2005).
34. Strausfeld, N. J. *Arthropod brains: evolution, functional elegance, and historical significance*. (Harvard University Press, 2012).
35. Maier-Hein, L. *et al.* Why rankings of biomedical image analysis competitions should be interpreted with care. *Nat. Commun.* **9**, 5217 (2018).
36. Robinson, G. E. Regulation of honey bee age polyethism by juvenile hormone. *Behav. Ecol. Sociobiol.* **20**, 329–338 (1987).
37. Waddington, K. D. Implications of variation in worker body size for the honey bee recruitment system. *J. Insect Behav.* **2**, 91–103 (1989).
38. Steijven, K., Spaethe, J., Steffan-Dewenter, I. & Härtel, S. Learning performance and brain structure of artificially-reared honey bees fed with different quantities of food. *PeerJ* **5**, e3858 (2017).
39. Haddad, D. *et al.* NMR imaging of the honeybee brain. *J. Insect Sci.* **4**, 1–7 (2004).
40. Mares, S., Ash, L. & Gronenberg, W. Brain allometry in bumblebee and honey bee workers. *Brain. Behav. Evol.* **66**, 50–61 (2005).
41. Maleszka, J., Barron, A. B., Helliwell, P. G. & Maleszka, R. Effect of age, behaviour and social environment on honey bee brain plasticity. *J. Comp. Physiol. A* **195**, 733–740 (2009).

42. Durst, C., Eichmüller, S. & Menzel, R. Development and experience lead to increased volume of subcompartments of the honeybee mushroom body. *Behav. Neural Biol.* **62**, 259–263 (1994).
43. Greco, M. K. & Stait-Gardner, T. Applying x-ray micro-tomography to learning and memory. *Biomed. Phys. Eng. Express* **3**, 024001 (2017).
44. Ribi, W., Senden, T. J., Sakellariou, A., Limaye, A. & Zhang, S. Imaging honey bee brain anatomy with micro-X-ray-computed tomography. *J. Neurosci. Methods* **171**, 93–97 (2008).
45. Prakash, Y. S., Smithson, K. G. & Sieck, G. C. Application of the Cavalieri principle in volume estimation using laser confocal microscopy. *NeuroImage* **1**, 325–333 (1994).
46. Barrett, M. *et al.* Neuroanatomical differentiation associated with alternative reproductive tactics in male arid land bees, *Centris pallida* and *Amegilla dawsoni*. *J. Comp. Physiol. A* **207**, 497–504 (2021).
47. Nowogrodzki, R. Division of labour in the honeybee colony: a review. *Bee World* **65**, 109–116 (1984).
48. Ismail, N., Robinson, G. E. & Fahrbach, S. E. Stimulation of muscarinic receptors mimics experience-dependent plasticity in the honey bee brain. *Proc. Natl. Acad. Sci.* **103**, 207–211 (2006).
49. Winnington, A. P., Napper, R. M. & Mercer, A. R. Structural plasticity of identified glomeruli in the antennal lobes of the adult worker honey bee. *J. Comp. Neurol.* **365**, 479–490 (1996).
50. Goulson, D. Bumblebees: behaviour, ecology, and conservation. *Bumblebees Behav. Ecol. Conserv.* (2010).
51. Rother, L. *et al.* A micro-CT-based standard brain atlas of the bumblebee. *Cell Tissue Res.* (2021) doi:10.1007/s00441-021-03482-z.
52. Austin, M. W. & Dunlap, A. S. Intraspecific variation in worker body size makes North American bumble bees (*Bombus* spp.) less susceptible to decline. *Am. Nat.* **194**, 381–394 (2019).
53. Spaethe, J. & Weidenmüller, A. Size variation and foraging rate in bumblebees (*Bombus terrestris*). *Insectes Sociaux* **49**, 142–146 (2002).
54. Letzkus, P., Boeddeker, N., Wood, J. T., Zhang, S.-W. & Srinivasan, M. V. Lateralization of visual learning in the honeybee. *Biol. Lett.* **4**, 16–19 (2008).
55. Letzkus, P. *et al.* Lateralization of olfaction in the honeybee *Apis mellifera*. *Curr. Biol.* **16**, 1471–1476 (2006).
56. Anfora, G. *et al.* Lateralization in the invertebrate brain: left-right asymmetry of olfaction in bumble bee, *Bombus terrestris*. *PLoS ONE* **6**, e18903 (2011).
57. Yang, E.-C., Lin, H.-C. & Hung, Y.-S. Patterns of chromatic information processing in the lobula of the honeybee, *Apis mellifera* L. *J. Insect Physiol.* **50**, 913–925 (2004).
58. Sahin, B. *et al.* Brain volumes of the lamb, rat and bird do not show hemispheric asymmetry: a stereological study. *Image Anal. Stereol.* **20**, 9 (2011).
59. Frasnelli, E., Vallortigara, G. & Rogers, L. J. Left–right asymmetries of behaviour and nervous system in invertebrates. *Neurosci. Biobehav. Rev.* **36**, 1273–1291 (2012).
60. Frasnelli, E. *et al.* The bee as a model to investigate brain and behavioural asymmetries. *Insects* **5**, 120–138 (2014).
61. Luders, E., Narr, K. L., Thompson, P. M. & Toga, A. W. Neuroanatomical correlates of intelligence. *Intelligence* **37**, 156–163 (2009).
62. Pietschnig, J., Penke, L., Wicherts, J. M., Zeiler, M. & Voracek, M. Meta-analysis of associations between human brain volume and intelligence differences: How strong are they and what do they mean? *Neurosci. Biobehav. Rev.* **57**, 411–432 (2015).
63. Lesciotto, K. M. *et al.* Phosphotungstic acid-enhanced microCT: optimized protocols for embryonic and early postnatal mice. *Dev. Dyn.* **249**, 573–585 (2020).
64. RStudio Team. RStudio: integrated development for R. RStudio, Inc., Boston, MA URL http://www.rstudio.com/. (2019).
65. Harrell, F. E. Hmisc: Harrell Miscellaneous. https://CRAN.R-project.org/package=Hmisc. (2020).
66. Bates, D., Mächler, M., Bolker, B. & Walker, S. Fitting linear mixed-effects models using lme4. *J. Stat. Softw.* **67**, 1–48 (2015).
67. Fox, J. & Weisberg, S. An {R} companion to applied regression, third edition. (2019).
68. Ronneberger, O., Fischer, P. & Brox, T. U-Net: Convolutional Networks for Biomedical Image Segmentation. in *Medical Image Computing and Computer-Assisted Intervention – MICCAI 2015* (eds. Navab, N., Hornegger, J., Wells, W. M. & Frangi, A. F.) vol. 9351 234–241 (Springer International Publishing, 2015).
69. Huang, G., Liu, Z., Van Der Maaten, L. & Weinberger, K. Q. Densely connected convolutional networks. in *2017 IEEE Conference on Computer Vision and Pattern Recognition (CVPR)* 2261–2269 (IEEE, 2017). doi:10.1109/CVPR.2017.243.

Acknowledgements

Three-dimensional data acquisitions were performed using the micro-CT facilities of the MRI platform member of the national infrastructure France-BioImaging supported by the French National Research Agency (ANR-10-INBS-04, «Investments for the future»), and of the Labex CEMEB (ANR-10-LABX-0004), and NUMEV (ANR-10-LABX-0020). We further acknowledge the support by the projects ASTOR (05K2013) and NOVA (05K2016) funded by the German Federal Ministry of Education and Research (BMBF), Informatics for Life funded by the Klaus Tschira Foundation, the state of Baden-Württemberg through bwHPC, the Ministry of Science, Research and the Arts Baden-Württemberg (MWK) through the data storage service SDS@hd, and the German Research Foundation (DFG; INST 35/1314-1 FUGG and INST 35/1134-1 FUGG). CM was funded by a PhD fellowship from the French Ministry of Higher Education, Research and Innovation. ML was funded by the Agence Nationale de la Recherche (3DNaviBee ANR-19-CE37-0024), the Agence de la Transition Ecologique (project LOTAPIS), and the European Commission (FEDER ECONECT MP0021763, ERC Cog BEE-MOVE GA101002644). We are grateful to Gergana Bozukova for improving the language of the manuscript.

Author contributions

P.D.L., C.M., R.L., J.-M.D., V.H. & M.L. conceived and designed the study. P.D.L. developed Biomedisa, devised algorithms and carried out the evaluation. C.M. performed original micro-CT scans, segmented the data, manually corrected and statistically analysed the segmentation results. A.J. developed AMIRA Mesh File reader. J.R. developed automatic cropping. V.H. & M.L. supervised the project. P.D.L. & C.M. wrote the first draft of the manuscript. All authors contributed to the writing and discussion.

Competing interests

The authors declare no competing interests.

Materials & Correspondence

Correspondence and requests for materials should be addressed to P.D.L. or C.M.

FIGURES AND TABLES

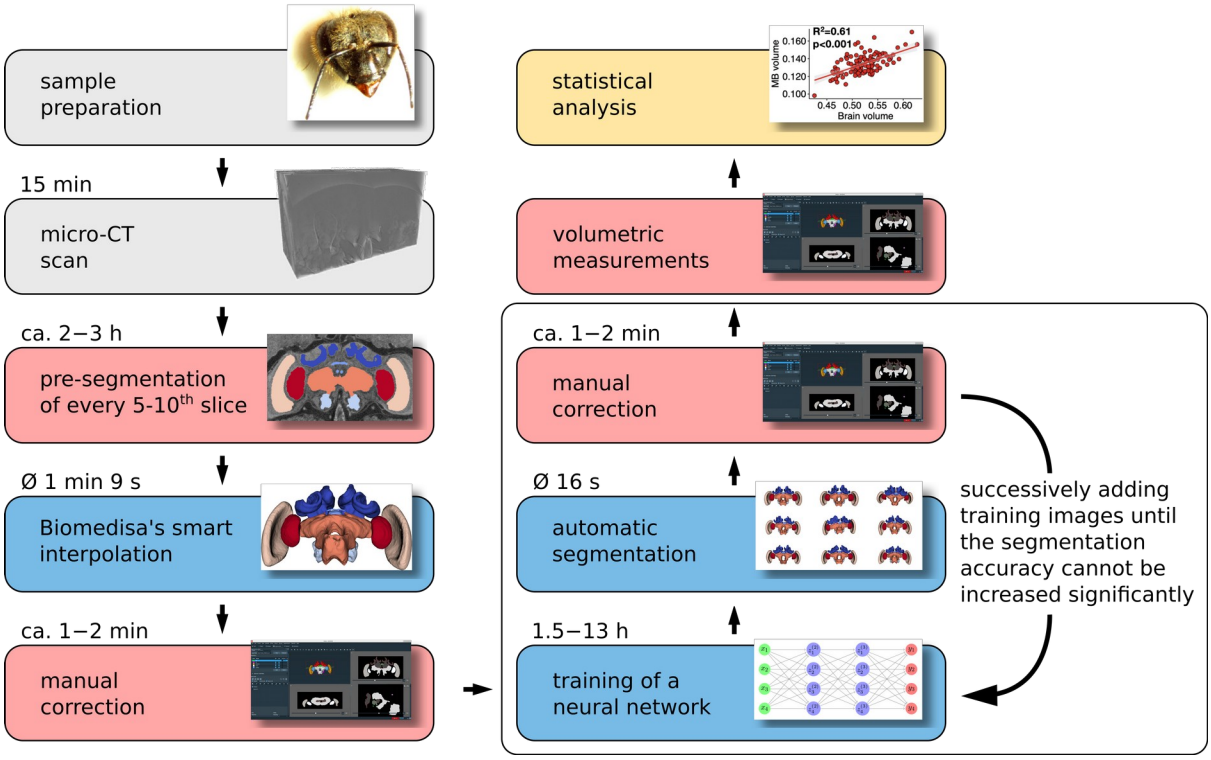

Fig. 1 Flowchart of the steps to perform large-scale quantitative comparative analyses of bee brain size and organisation using micro-CT imaging and the Biomedisa segmentation platform. After sample preparation and volume reconstruction (grey boxes), the micro-CT scans are segmented with AVIZO 2019.1 (red boxes) in combination with Biomedisa (blue boxes). The volumes are then measured with AVIZO 2019.1 and statistically analysed with R Studio (yellow box).

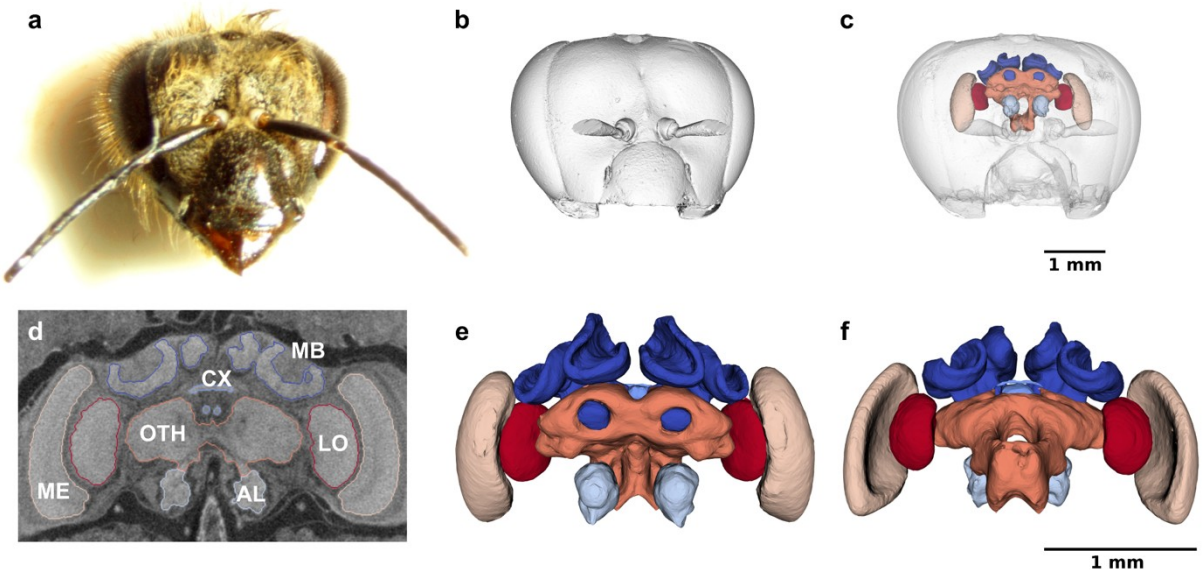

Fig. 2 Surface renderings of an example of CT-scanned honey bee head and reconstructed brain neuropils. a Frontal view of the head of a forager bee (ID 79, hive H4). **b** Surface rendering of the head with the mandibles removed. **c** Overlay of the head and reconstructed neuropils. **d** Frontal cross-section of the tomogram with the segmentation boundaries of the mushroom bodies (MB), central complex (CX), antennal lobes (AL), medullae (ME), lobulae (LO) and other neuropils (OTH). **e** Frontal view of the reconstructed MB (*dark blue*), CX (*sky blue*), AL (*light sky blue*), ME (*beige*), LO (*red*) and OTH (*orange*). **f** Dorsal view of the reconstructed neuropils. b, c, e and f created with ParaView Glance integrated in Biomedisa's online platform.

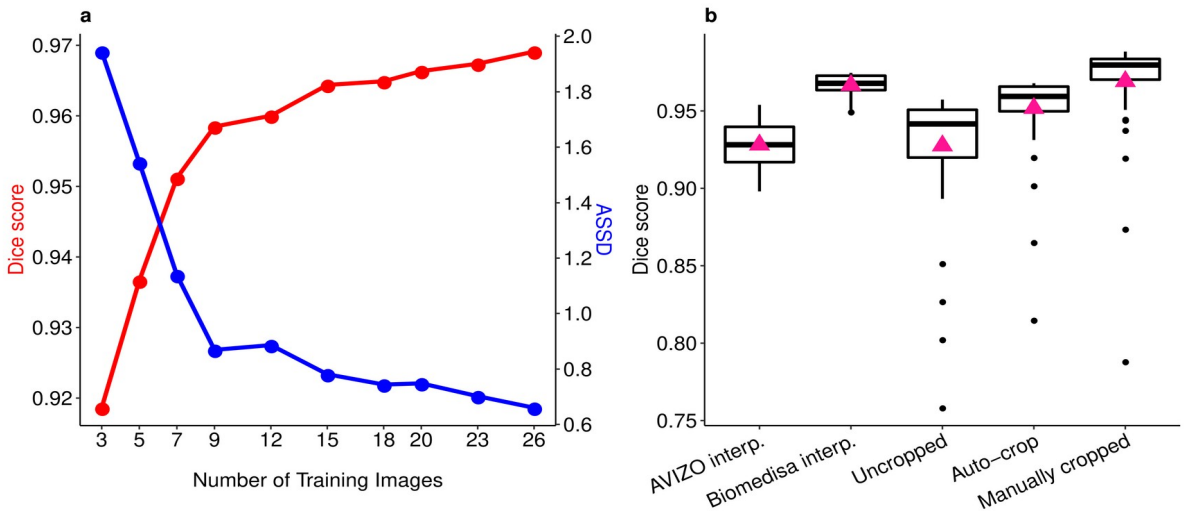

Fig. 3 Segmentation accuracy of Biomedisa's semi-automatic and automatic segmentation of honey bee CT scans. a Average Dice scores and ASSD of the automatic segmentation results for an increasing number of training images. **b** Semi-automated segmentation accuracy (Dice score) of the AVIZO interpolation and the Biomedisa interpolation as well as segmentation accuracy of the automatic segmentation for uncropped image data, using Biomedisa's auto-copping and manually cropped image data. Boxplots show median volumes (intermediate line) and quartiles (upper and lower lines). Pink triangles display mean volumes. For performance tests of the automatic segmentation, the 84 honey bee test images were split into 30 validation images and 54 test images (see "Methods").

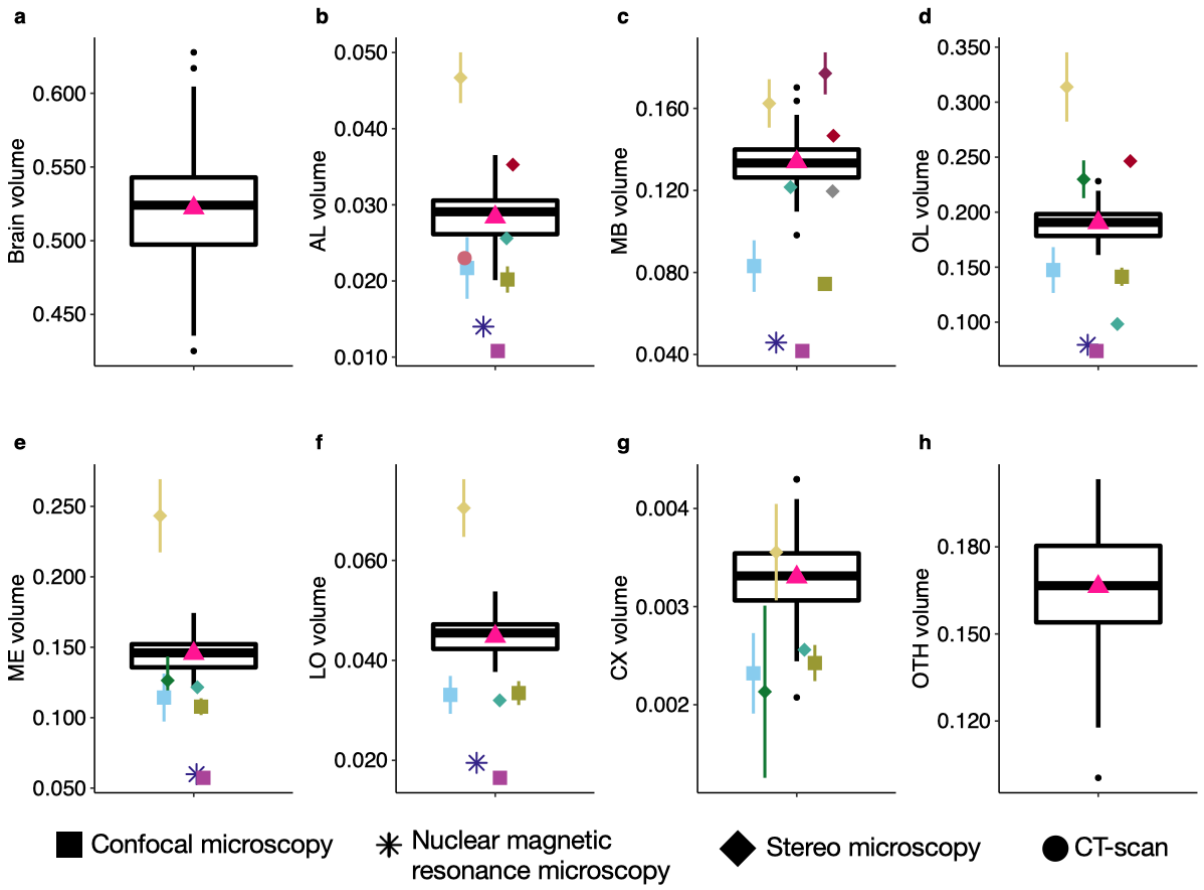

Fig. 4 Variation in brain and neuropils volumes (mm³) for honey bees (N=110). a Total brain. **b** Antennal lobes (AL). **c** Mushroom bodies (MB). **d** Optic lobes (OL). **e** Medullae (ME). **f** Lobulae (LO). **g** Central complex (CX). **h** Other neuropils (OTH). Boxplots show median volumes (intermediate line) and quartiles (upper and lower lines). Pink triangles display mean volumes. Coloured symbols show mean (± s.d. when available) of neuropil volumes described for forager honey bees in other studies: using confocal microscopy (*square*): Brandt et al.[33] (N=20 bees - *light blue*); Steijven et al.[38] (N=10 - *kaki*); Haddad et al.[39] (*purple*); using nuclear magnetic resonance microscopy (*star*): Haddad et al.[39] (N=8 - *deep blue*); using stereo microscopy (*diamond*): Gowda & Gronenberg[31] (N=7 - *yellow)*; Gronenberg & Couvillon[32] (N=121 European and Africanized honey bees - *dark green*); Mares et al.[40] (N=25 - *turquoise*); Maleszka et al.[41] (N=30 - *burgundy*); Withers et al.[27] (*red*); Durst et al.[42] (N=12 - *grey*); using CT scan (*point*): Greco and Stait-Gardner[43] (N=10 - *coral*). For the total brain volume, comparisons with other studies are not shown because of the cumulative uncertainties of the measurements.

Table 1 Total brain and neuropil volumes of honey bees (N=110). Mean (± standard deviation), minimal and maximal volumes (mm³) and percentage of volume variation ((Max-Min)*100/Max). For paired neuropils, detailed data for both sides (left/right) are given. Note that the left/right comparison for MB is based on data from 59 honey bees only, as some bees have both sides merged in the automatic segmentation result. F-test, following LMMs, tests the significance of the fixed variable 'hive', and results are displayed in bold when significant.

Volume (mm³)	Mean ± s.d.	Min	Max	% variation	F-test
Brain	0.522±0.038	0.425	0.628	32.27%	F(8,101)=1.018, p=0.428
AL	0.0284±0.0033	0.0201	0.0365	44.97%	**F(8,101)=5.055, p<0.001**
Left	*0.0141±0.0018*	*0.0096*	*0.0182*	*47.49%*	
Right	*0.0142±0.0017*	*0.0095*	*0.0183*	*47.76%*	
MB	0.134±0.011	0.098	0.170	42.30%	**F(8,101)=2.315, p=0.025**
Left	*0.065±0.005*	*0.048*	*0.073*	*34.26%*	
Right	*0.066±0.007*	*0.030*	*0.075*	*60.25%*	
OL	0.190±0.014	0.161	0.228	29.41%	**F(8,101)=4.368, p<0.001**
Left	*0.095±0.007*	*0.080*	*0.116*	*31.29%*	
Right	*0.095±0.007*	*0.082*	*0.112*	*27.46%*	
ME	0.146±0.011	0.122	0.174	29.95%	F(8,101)=2.819, p=0.288
Left	*0.073±0.005*	*0.060*	*0.089*	*32.29%*	
Right	*0.073±0.006*	*0.062*	*0.085*	*27.52%*	
LO	0.045±0.004	0.038	0.054	29.94%	**F(8,101)=2.733, p=0.009**
Left	*0.0224±0.002*	*0.0185*	*0.027*	*30.72%*	
Right	*0.0223±0.002*	*0.0179*	*0.027*	*33.96%*	
CX	0.0033±0.0004	0.0021	0.0043	51.74%	F(8,101)=1.839, p=0.400
OTH	0.166±0.019	0.100	0.203	50.61%	F(8,101)=1.643, p=0.433

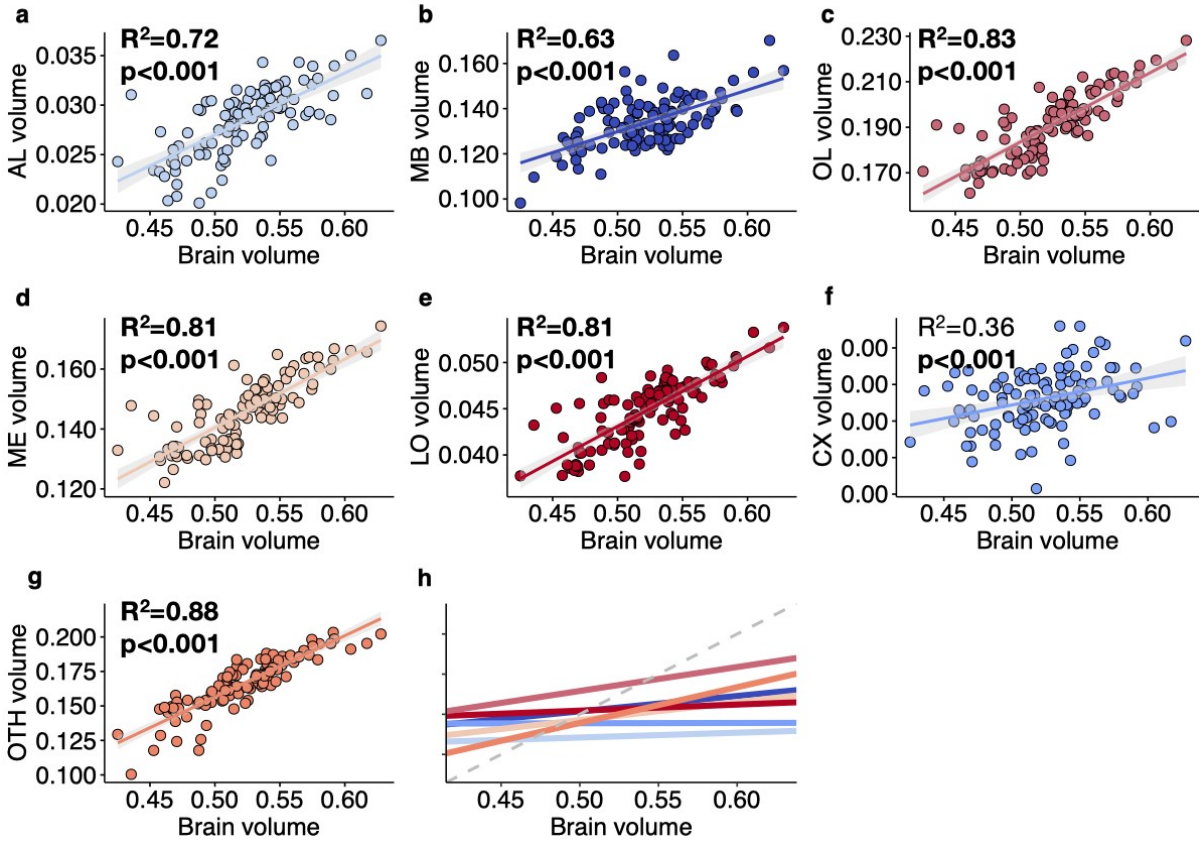

Fig. 5 Correlation between neuropil volumes and total brain volume (mm^3) (N=110 honey bees). **a** Antennal lobes (AL). **b** Mushroom bodies (MB). **c** Optic lobes (OL). **d** Medullae (ME). **e** Lobulae (LO). **f** Central complex (CX). **g** Other neuropils (OTH). Regression lines displayed with 95% confidence intervals. Pearson correlation coefficient (R^2) and p-value are given. Strong correlations (R^2>0.40) and significant correlations (p<0.05) are displayed in bold. **h** Linear correlations for the different neuropils (y-axis not given: differs for each neuropil). Grey broken line indicates true isometric correlation (slope=1).

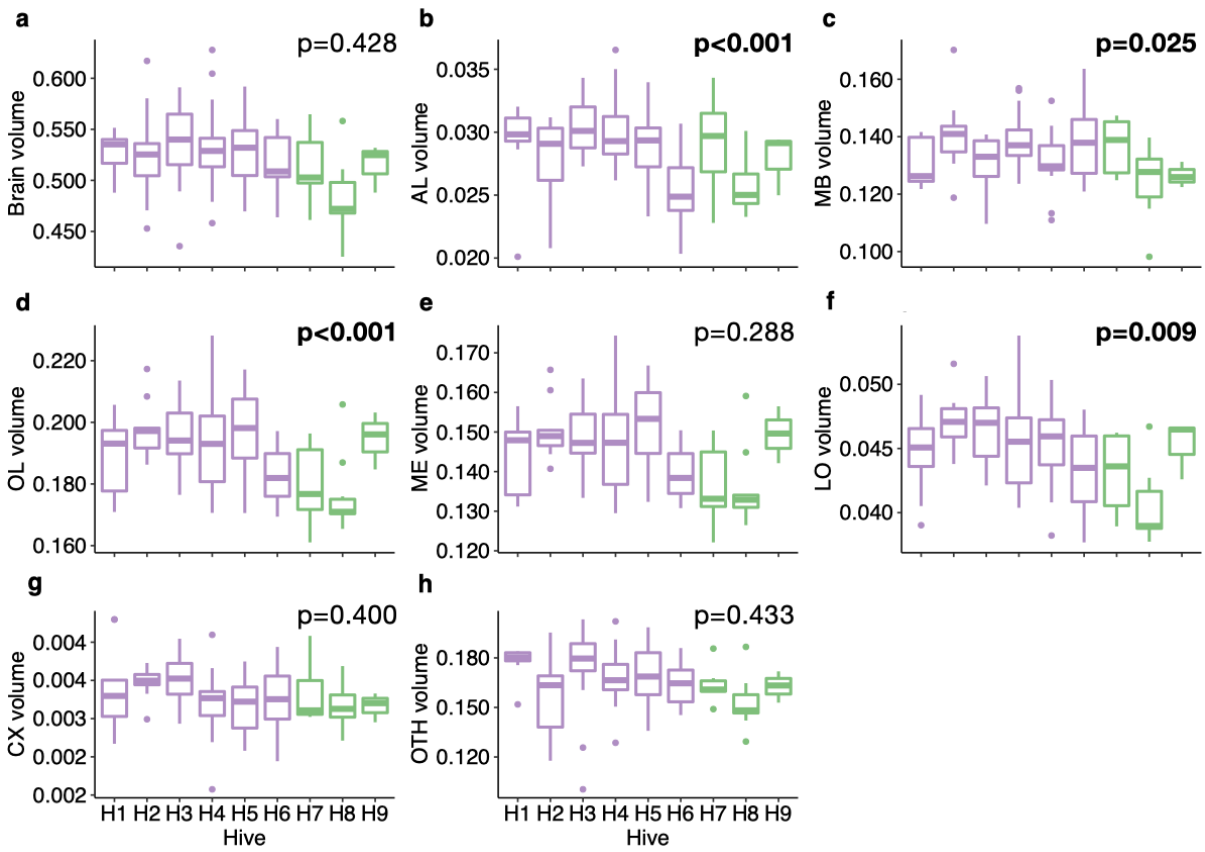

Fig. 6 Variation in brain volume and absolute volume of neuropils (mm^3) between honey bee colonies (population A - *purple*, N=6 hives; population B - *green*, N=3 hives). a Total brain. **b** Antennal lobes (AL). **c** Mushroom bodies (MB). **d** Optic lobes (OL). **e** Medullae (ME). **f** Lobulae (LO). **g** Central complex (CX). **h** Other neuropils (OTH). Statistical comparisons (p-values) for the neuropil volumes between hives were obtained from the F-test following LMMs and are displayed in bold when significant (statistical details in Table 1).

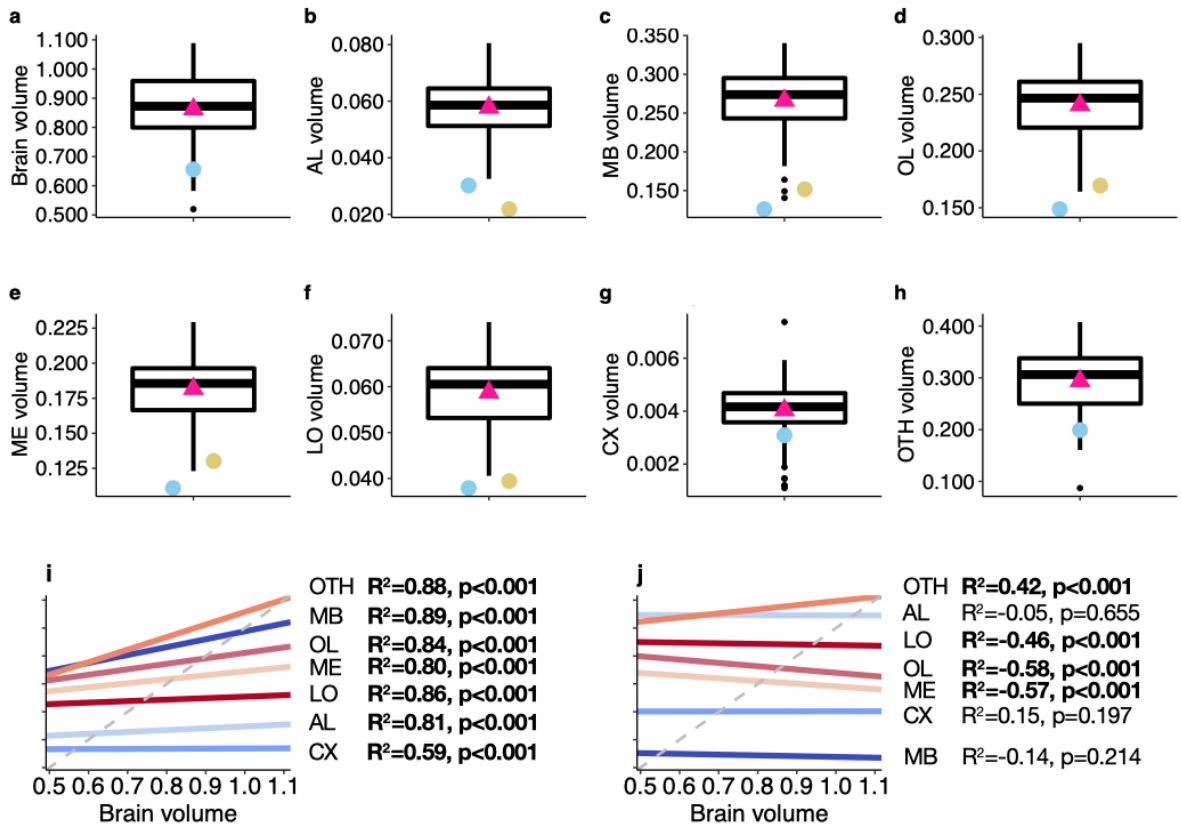

Fig. 7 Variation in brain volume and neuropils volumes (mm^3) and correlation between neuropil volumes and total brain volume for bumblebees (N=77). a Total brain. **b** Antennal lobes (AL). **c** Mushroom bodies (MB). **d** Optic lobes (OL). **e** Medullae (ME). **f** Lobulae (LO). **g** Central complex (CX). **h** Other neuropils (OTH). Boxplots show median volumes (intermediate line) and quartiles (upper and lower lines). Pink triangles display mean volumes. Coloured symbols show mean of neuropils volumes described for bumblebees in other studies using CT-scan: Rother et al.[51] (N=10 bees - *light blue*), Smith et al.[17] (N=38 bees - *yellow*). **i** Linear correlations between absolute volumes of neuropils and total brain volume (mm^3) (y-axis not given: differs for each neuropil). **j** Linear correlations between relative volumes of neuropils and total brain volume (mm^3) (y-axis not given: differs for each neuropil). Grey broken line indicates true isometric correlation (slope=1). Pearson correlation coefficient (R^2) and p-value are given. Strong correlations (R^2>0.40) and significant correlations (p<0.05) are displayed in bold.

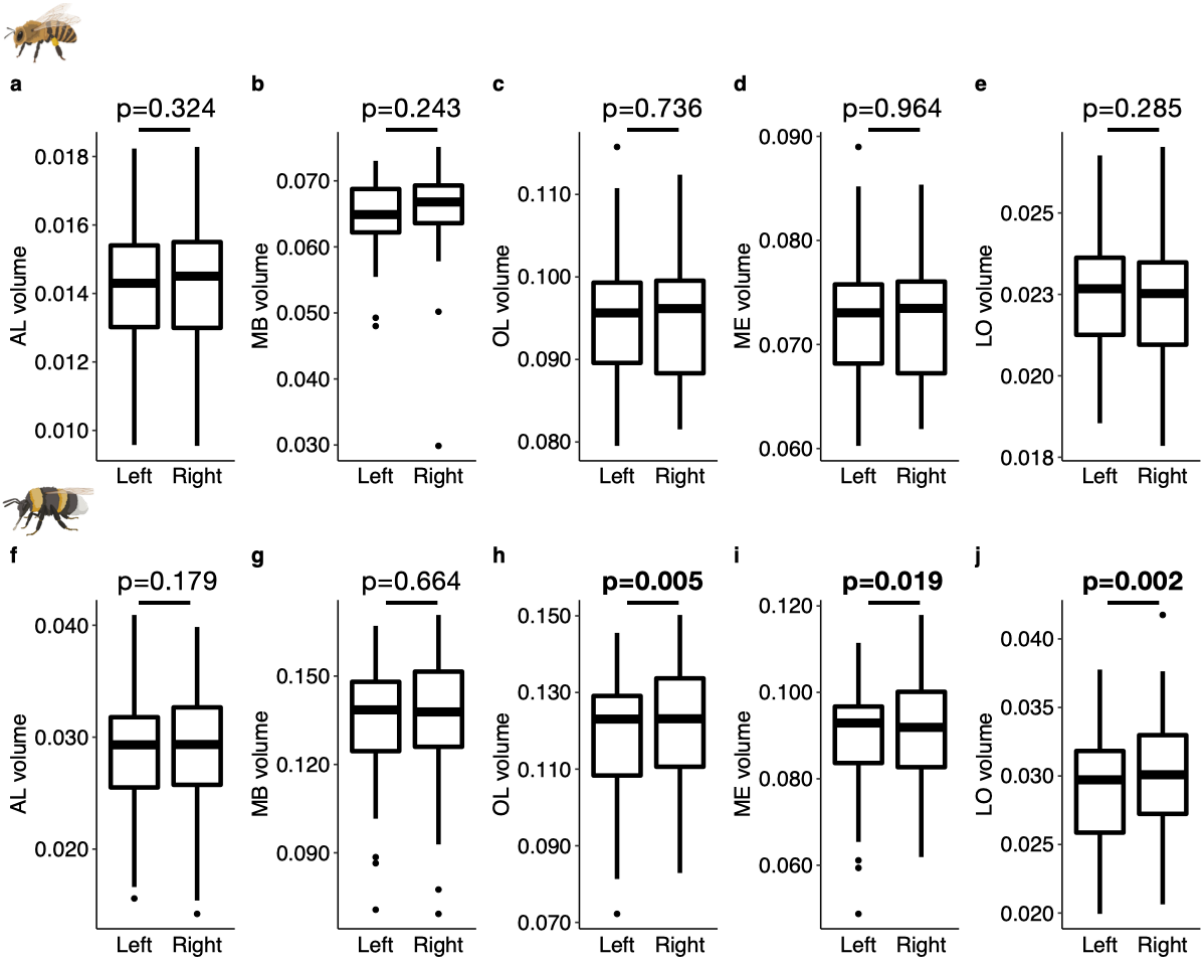

Fig. 8 Comparisons between left and right volumes (mm^3) for paired neuropils in honey bees (N=110; a−e) and bumblebees (N=77; f−j). a, f Antennal lobes (AL). **b, g** Mushroom bodies (MB). **c, h** Optic lobes (OL). **d, i** Medullae (ME). **e, j** Lobulae (LO). Boxplots show median volumes (intermediate line) and quartiles (upper and lower lines). Statistical differences (p-values) for the neuropil volume between left and right side were obtained with Student's t-Test, and are displayed in bold when significant.